

Coupling of tribovoltaic effect and tribo-electrostatic effect at dynamic semiconductor heterojunction interfaces[☆]

Jia Meng^{a,b,c,d}, Chuntao Lan^d, Chongxiang Pan^{a,b,c,d}, Guoxu Liu^{d,e},
Xiong Pu^{a,b,c,d,e,*}, Chi Zhang^{a,b,c,d,e,*}, Zhong Lin Wang^{d,e,f}

^a School of Physical Science & Technology, Guangxi University, Nanning 530004, China

^b Key Laboratory of Blue Energy and Systems Integration (Guangxi University), Education Department of Guangxi Zhuang Autonomous Region, Nanning 530004, China

^c Center on Nanoenergy Research, Institute of Science and Technology for Carbon Peak & Neutrality, Guangxi University, Nanning 530004, China

^d CAS Center for Excellence in Nanoscience, Beijing Key Laboratory of Micro-nano Energy and Sensor, Beijing Institute of Nanoenergy and Nanosystems, Chinese Academy of Sciences, Beijing 101400, China

^e School of Nanoscience and Engineering, University of Chinese Academy of Sciences, Beijing 100049, China

^f Guangzhou Institute of Blue Energy, Knowledge City, Huangpu District, Guangzhou 510555, China

ARTICLE INFO

Keywords:

Tribovoltaic effect
Electrostatic induction effect
Tribovoltaic nanogenerator
Semiconductor heterojunction

ABSTRACT

Tribovoltaic effect at the dynamic semiconductor interface is of great fundamental and practical importance for developing a variety of functional devices; yet, it can be coupled with a series of different physical effects, such as the contact-electrification induced electrostatic effect and mechanical wearing effect, and the coupling mechanisms are still remained to be elucidated. Herein, we investigated the coupling between tribovoltaic and tribo-electrostatic effects at the dynamic heterojunctions of two wide-bandgap semiconductors: zinc oxide (ZnO) and gallium nitride (GaN). It is found that, in the contact-separation mode, the direct-current outputs from tribovoltaic effect can be clearly distinguished from the alternating-current outputs from tribo-electrostatic effect. Then, humidity, external load resistance and pressure force are found to reveal the coupling characteristics of these two effects, that tribovoltaic outputs are less affected by humidity, show smaller matched impedance and are more sensitive to high pressure force, diverging from the tribo-electrostatic outputs. Lastly, we demonstrate that the mechanical wearing effect can be inhibited in contact-separation mode, achieving long-term stability over 50,000 cycles. Therefore, this work provides insights to the mechanism of tribovoltaic effects and practical guidance for high-performances tribovoltaic devices.

1. Introduction

The interface physics of semiconductors is the fundamentals for developing various functional devices[1,2], but the dynamic interface of semiconductors has not been widely studied until the very recent discovery of tribovoltaic effect[3–5]. The tribovoltaic effect refers to the electricity generation phenomenon at the dynamic semiconductor interfaces, where the electron-hole pairs are excited by the energy release

during friction and then are separated by the built-in electric field at the junctions, outputting the observed direct-current electricity to the external circuit.[3,5] This electron excitation process differs from photo-excitation and is probably due to the transition of electrons between the surface states during contact or bond formation across the sliding interface. Based on this effect, a variety of tribovoltaic nanogenerators (TVNG) have been developed to covert kinetic energy into electricity[6], which have great potentials in realizing self-powered

[☆] Prof Zhong Lin Wang, an author on this paper, is the Editor-in-Chief of Nano Energy, but he had no involvement in the peer review process used to assess this work submitted to Nano Energy. This paper was assessed, and the corresponding peer review managed by Professor Chenguo Hu, also an Associate Editor in Nano Energy

^{*} Corresponding authors at: School of Physical Science & Technology, Guangxi University, Nanning 530004, China.

^{**} Corresponding author at: CAS Center for Excellence in Nanoscience, Beijing Key Laboratory of Micro-nano Energy and Sensor, Beijing Institute of Nanoenergy and Nanosystems, Chinese Academy of Sciences, Beijing 101400, China.

E-mail addresses: puxiong@binn.cas.cn (X. Pu), czhang@binn.cas.cn (C. Zhang), zlwang@binn.cas.cn (Z.L. Wang).

<https://doi.org/10.1016/j.nanoen.2024.110395>

Received 16 August 2024; Received in revised form 16 October 2024; Accepted 20 October 2024

Available online 23 October 2024

2211-2855/© 2024 Elsevier Ltd. All rights are reserved, including those for text and data mining, AI training, and similar technologies.

devices or energy-autonomous systems[7]. The TVNG has the advantages including the high DC density and power density outputs, the low internal impedance, and the facile structure design, diverging from the alternating-current (AC) outputs with high internal impedance of triboelectric nanogenerators (TENG) based on the electrostatic induction effect of tribo-static charges[8]. Recently, the TVNG has experienced rapid progresses on both the fundamental mechanisms and device performances[9–11]. For the former aspect, “bindingtons”, the quantized energy generated during interfacial binding/debinding processes [12,13], have been proposed to account for the electron excitation with

mechanical energy input. For the latter aspect, the electrical outputs have been found to be dramatically improved by the optimization of enlarged Fermi energy level difference of the interface[14,15], the introduced ferroelectric polarization field[16], the appropriate doping of the semiconductors, and so on. Also, the durability of the TVNG has been significantly improved by introducing interface lubricants[17,18], utilizing rolling friction rather than sliding friction[19,20], or designing the device into contact-separation mode[21]. One important finding demonstrated that the voltage of a TVNG can be boosted up to about 130 V by the sliding friction at wide-bandgap semiconductor GaN[22].

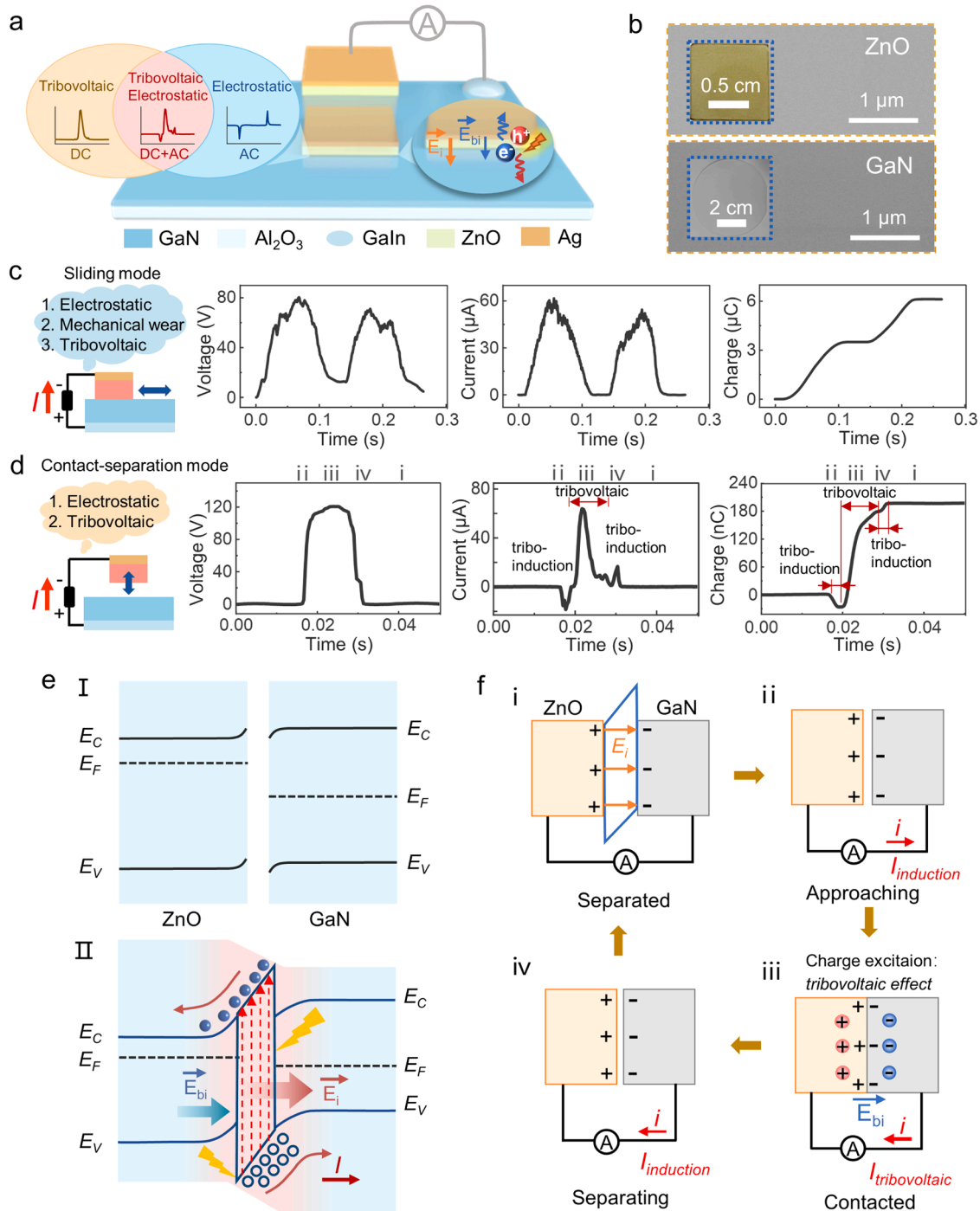


Fig. 1. Structural and electrical output characteristics of the heterojunction generator. (a) 3D schematic of the generator. (b) SEM images of ZnO (top) and GaN (bottom). (c and d) Open-circuit voltage, short-circuit current, and transferred charges output characteristics of the generator in (c) sliding mode and (d) contact-separation mode. (e) Energy band diagrams of ZnO and GaN before contact and after sliding or contact-separation. (f) Electrical output coupling tribovoltaic effect and tribo-electrostatic effect in contact-separation mode.

Then, this dramatically increased voltage has been attributed to the field generated by the accumulated static charges owing to contact-electrification at the GaN interface, which coupled with the built-in electric field and contributed to the charge excitation and separation. The charge carriers are generated by the tribovoltaic effect, and the tribo-electrostatic charges results in the enhanced output voltage. Therefore, this coupling between electrostatic and tribovoltaic effects suggests a promising approach to improve the electrical outputs of TVNGs.

Friction is a ubiquitous phenomenon, which actually could couple a series of different physical or chemical effects, such as the mechanical wearing, mechanochemistry, triboelectrification and tribovoltaic effects.[23,24] As for a TVNG, some of these effects could positively contribute to the electricity outputs, whereas some others could be detrimental. For instance, the undesirable mechanical wearing effect is better to be inhibited for promoted durability[25,26]; yet, the observed coupling between electrostatic and tribovoltaic effects could enhance the electrical outputs[27,28]. Therefore, it is essential to understand the coupling mechanism of these possible effects at dynamic semiconductor interfaces, so as to provide guidance for the development of high-voltage, high-current and long-durability TVNGs.

Herein, we propose to study the coupling mechanisms between tribovoltaic and electrostatic effects of a TVNG based on the semiconductor dynamic heterojunction of two wide-bandgap semiconductors, i.e. zinc oxide (ZnO) and gallium nitride (GaN). We found that the electrical outputs originated from these two effects could be clearly distinguished under the contact-separation-mode. Then, the DC tribovoltaic outputs and AC tribo-electrostatic outputs can be tuned through the environmental humidity and external load resistances. High humidity significantly diminished the AC outputs due to electrostatic leakage, while the DC outputs remained less affected. Additionally, electrostatic induction and tribovoltaic effect exhibited different internal impedance with diverged matched impedance. External pressure force could promote the outputs of both the two effects, but with a stronger effect on the tribovoltaic outputs at high pressure. Finally, we demonstrated that the mechanical wearing effect can be inhibited in contact-separation mode, achieving long-term cycle stability over 50,000 cycles.

2. Result and discussion

2.1. Structure and electrical output characteristics

As illustrated in Fig. 1a, at the dynamic interfaces of wide-bandgap semiconductors, there could be coupled electrostatic and tribovoltaic effects. In particular for the undoped semiconductors with high resistivity, the static charges could not be easily dissipated and would accumulate at the surfaces.[22] Then, both the electrostatic electric field and the built-in electric field at the heterojunctions could contribute to the charge excitation and separation processes.[27] In this work, to study the coupling between electrostatic and tribovoltaic effects, a heterojunction TVNG was fabricated by using two wide-bandgap semiconductor materials, i.e. ZnO and GaN (Fig. 1a). The TVNG will be studied based on both the contact-separation mode and sliding friction mode. We found that the electrical signals generated from electrostatic induction and tribovoltaic effects can be clearly distinguished in the contact-separation mode, respectively, in contrast to the merged signals in sliding mode. The detailed specifications and conductivities of involved intrinsic GaN (Gallium Nitride) and ZnO crystals are shown in Table S1. The scanning electron microscopy (SEM) images of ZnO single crystal bulk and GaN grown on sapphire substrate are shown in Fig. 1b, both with delicately smooth surfaces. Schematic diagrams of the GaN crystal structure and the hexagonal wurtzite ZnO crystal structure are shown in Fig. S1, both oriented along the [0001] crystal orientation. The Ohmic contacts both between ZnO and Ag, GaN and GaIn alloy (Fig. S2) were confirmed, so the Ag and GaIn alloy were selected as the two

electrodes for TVNGs. The current-voltage (I - V) curves of GaN/ZnO heterojunctions indicated that the built-in electric field direction in the GaN/ZnO heterojunction is pointing from ZnO to GaN (Fig. S3).

For testing the outputs of TVNG, the positive terminal of an electrometer was connected to GaIn/GaN and the negative terminal was connected to Ag/ZnO. Comparing the profiles of electrical signals obtained from the TVNG operating in sliding and contact-separation modes, significant differences can be clearly observed. As for each sliding motion, a broad peak of open-circuit voltage and short-circuit current can be generated, and the transferred charge accumulates stepwise (Fig. 1c). At a contact force of 60 N and a relative humidity (RH) of 10 %, the open-circuit voltage, short-circuit current and transferred charges per cycle is 80.4 V, 61.6 μ A, and 3.5 μ C, respectively. In contrast, a pair of AC peaks can be obtained together with another broad DC peak for contact-separation mode (Fig. 1d). This pair of AC signals is accordant with the events of approaching and separating motion, respectively, while the broad DC peak occurs during the contact period. Accordingly, the profile of transferred charge per cycle can be associated with the three current peaks, where the charges can also accumulate stepwise but a slight transient dip can be clearly observed in each step. The voltage profile is kind of merged together, but a shoulder peak can still be distinguished. Therefore, in contact-separation mode, the AC signals from the electrostatic induction effect and the broad DC signals from the tribovoltaic effect can be clearly distinguished, which offers the opportunity to study their coupling effects. At the same contact force and humidity, the TVNG generated an exceptionally high open-circuit peak voltage of 120.8 V. It is noted that there is an accumulation period for the electrostatic charges, during which the voltage increases and gets to the saturation after about 45 contact-separation cycles, as shown in Fig. S4. Here, the humidity was also intentionally controlled to be as low as RH 10 % to enhance the electrostatic induction effect and intrinsic undoped GaN was used as well. The peak value of AC current is about 18.4 μ A, and the peak DC current is about 63.8 μ A. The transferred AC charge per cycle is 26.3 nC, while the DC charge is 197.1 nC.

To further confirm the existence of electrostatic induction effect and exclude the possible piezoelectric effect, a series of control experiments were conducted. A single-electrode generator with only the ZnO/Ag grounded can generate characteristic AC signals correspond to a single-electrode TENG, confirming the presence of electrostatic charges at the ZnO/GaN interfaces (Fig. S5). Meantime, the TVNG operates in non-contact approaching-separating mode can output AC signals but orders of magnitude lower peak values, which also supports the existence of electrostatic induction effect (Fig. S6). To evaluate the piezoelectric effect, the output of ZnO and GaN in repeated compression mode is only about mV and nA scale (Fig. S7). Also, by comparing the ZnO [0001] crystal with two other non-polar crystal orientations, the output of TVNG shows no noticeable variations (Fig. S8, S9). Therefore, these evidences strongly support that the piezoelectric effect at the heterojunction is negligible.

2.2. Working mechanism

The electronic structure of ZnO and GaN is crucial for understanding the tribovoltaic effect. Based on the band gap and UPS spectrum (Fig. S10), the work function, conduction band, and valence band of ZnO are approximately 4.0 eV, 3.86 eV, and 7.16 eV, respectively.[29] For GaN, these values are approximately 4.8 eV, 3.1 eV, and 6.5 eV, respectively.[30] As the Fermi level of ZnO is higher than that of GaN (Fig. 1e (I)), higher-energy electrons in ZnO can diffuse into GaN when they are in contact, leaving positively charged cations fixed in the ZnO crystals and forming a space charge region at the heterojunction. Then, there will establish a built-in electric field (E_{bi}) pointing from the ZnO to the GaN in the space charge region. Meantime, the contact or sliding between ZnO and GaN also could lead to another electrification effect, that surface electrostatic charges could be generated. As confirmed by a Faraday cage testing (Fig. S11), there will be electrostatic positive

charges on the surface of ZnO and negative charges on the surface of GaN after they sliding with each other. As both the ZnO and GaN are undoped and have high resistivity, these surface electrostatic charges cannot be easily dissipated, other than the air breakdown leakage. Therefore, these surface electrostatic charges will lead to the formation of an interface electric field, which can be orders of magnitude higher than the built-in electric field. As these two electric fields are in the same direction in our case, they could be coupled to contribute to the tribovoltaic electricity generation processes. As illustrated in the Fig. 1e (II), when the electrons are excited by mechanical energy, the generated non-equilibrium electrons and holes will be separated by the coupled built-in electric field and the interface electric field, which accounts for the high voltage obtained from the TVNG. Also, this coupled field can also enhance the charge separation to enlarge the tribovoltaic current.

During contact-separation motions, a detailed charge excitation and separation process of a TVNG is illustrated in Fig. 1f. After several contact cycles, the electrostatic charges will be accumulated on the surfaces of ZnO and GaN (stage i). When they are approaching together, electrostatic induction occurs between the two semiconductors and electrodes to generate an induction current in external circuits (process ii). When ZnO and GaN are in deep contact (process iii), a built-in electric field is established pointing from ZnO to GaN. Simultaneously, electron cloud overlaps among the interface atoms with dangling bonds could releasing energies, which, in turn, could excite electrons and generate non-equilibrium electron-hole pairs. The excited electron-hole pairs at the interface will then be separated by the built-in electric field,

thereby forming a DC output in the external circuit. When separating ZnO and GaN (process iv), electrostatic induction arises again, leading to another induction current pulse in the direction opposite to the previous one. When the two are completely separated (process i), the induction current diminishes and the interface electric field would be established due to the existence of surface static charges on ZnO and GaN. As the electrostatic induction and tribovoltaic processes take place in different time domain, they can be distinguished clearly from the current signals.

2.3. Coupling characteristics

Considering the different characteristics of the tribovoltaic and electrostatic effects, they can be decoupled through a series of approaches. First, the influences of the environmental humidity on these two effects could be different. It is well known that humidity seriously affects the output performances of TENGs[31,32]. The output performances of TENGs usually decrease significantly in high humidity air [33], and the surface electrostatic charge accumulation could be suppressed[34,35]. Whereas, the tribovoltaic outputs could be less affected by the humidity. Therefore, the outputs of the heterojunction TVNG in contact-separation mode was observed in different humidity environments. To see the periodicity of the voltage and current signals, two consecutive voltage/current signals are shown in Fig. S12. At a contact force of 60 N (Fig. 2a), the voltage decreases from ~121 V to ~61 V as RH increases from 10 % to 60 %, then stabilizes at ~54 V at RH of 70–90 %, and then decreases to ~35 V at RH of 95 %. The

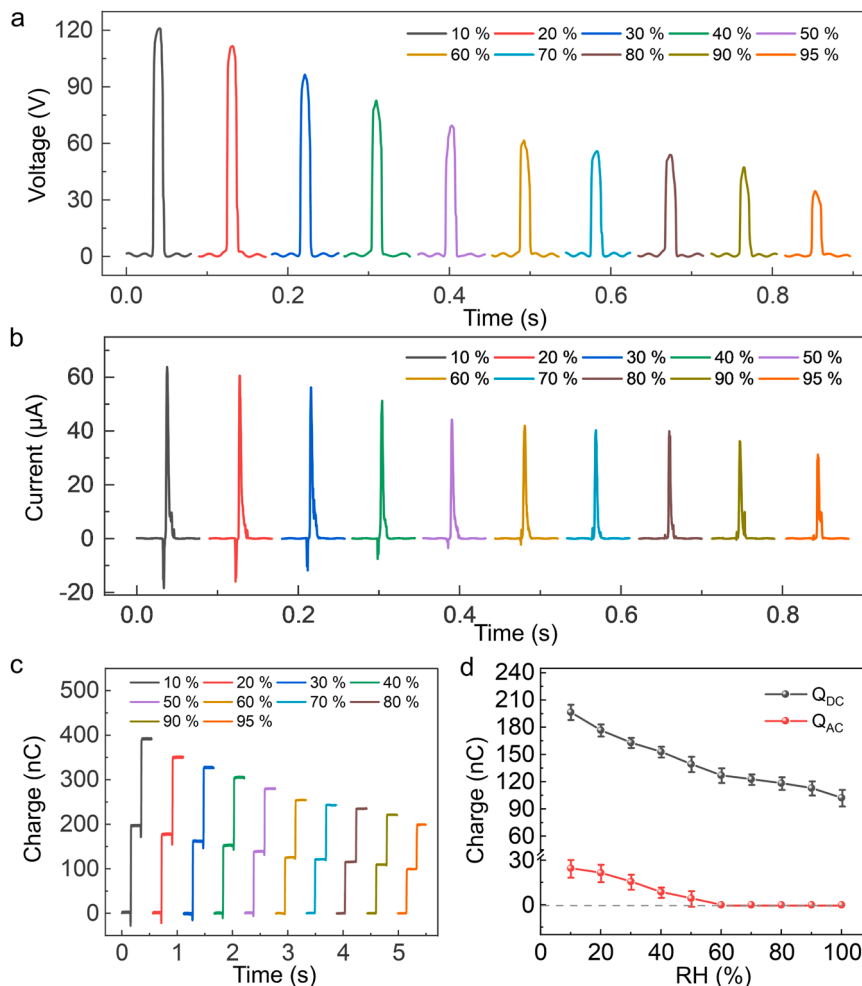


Fig. 2. Coupling characteristics under different humidity. (a) Open-circuit voltage and (b) short-circuit current of the generator under different humidity. (c) Transferred charge curves and (d) statistics of DC and AC charges of the generator under different humidity.

corresponding positive tribovoltaic current drops from 64 μA to 42 μA , stabilized at 40 μA , and drops to $\sim 31 \mu\text{A}$ (Fig. 2b). In comparison, the AC current arising from the electrostatic induction effect decreases dramatically from 18.4 μA at RH 10 % to 2.3 μA at RH 50 %, and then decay to be negligible at RH above 60 %, attributed to leakage of surface static charges and electrostatic charge cannot be accumulated in a high humid environment. This trend can also be verified from the charge curve. A decreasing dip can be observed when RH is lower than 50 % in each charge step, but it disappears when RH is above 60 % (Fig. 2c). It is worth noting that the charge curve is measured directly, which is consistent with the charge obtained by the integral of the measured current (Fig. S13). The average DC charge transferred per cycle due to the tribovoltaic effect is attenuated from 196.6 nC (RH 10 %) to 127.1 nC (RH 60 %) and remains near 118.4 nC (RH 90 %). In contrast, AC induction charge significantly drops to zero at RH 60 % (Fig. 2d). Therefore, it is strongly supported that the electricity generation by electrostatic induction effect could be decreased when increasing humidity, and even be eliminated at RH over 60 %. Nevertheless, it should be emphasized that the tribovoltaic electricity generation also decreases with humidity, even though it stabilizes at high humidity environment. This trend supports that the interface electric field associated with the surface electrostatic charges couples with the built-in electric field to enhance the tribovoltaic current generation in dry environment.

Another different characteristic between the electrostatic induction and the tribovoltaic effects is their different internal impedance. It is

known that based on the capacitor model, the power delivered by the TENG to the external loading resistor is determined by the internal impedance, the actual change in capacitance between the two electrodes (C), the parasitic capacitance and the external resistance (R). [36] Due to the slow charging process, a larger R will also suppress the displacement current of the TENG [37]. Therefore, it is possible to observe the distinctive effects on the output electrical signals by varying the external loading resistances. At a contact force of 60 N and a relative humidity of 20 %, the output voltage on the loading resistor (R_L) increases as R increases, while the corresponding short-circuit current decreases (Fig. 3a, b). The voltage, current and charge peaks on the load are perfectly aligned and consistent when the generator is connected to a resistance of 5 M Ω (Fig. S14) and 10 M Ω (Fig. S15). Specifically, when R reaches 10 M Ω , the negative voltage is significantly reduced, and negative current nearly disappears, showing only positive voltage and current. The transferred charge curve exhibits a step-like shape, with ~ 28.2 nC per motion cycle (Fig. 3c). The trend in the average charges of DC and AC as a function of R is presented in Fig. 3d. The DC charge drops rapidly from 120.2 nC to 39.2 nC (R of 1 k Ω to 5 M Ω) and then continues to decrease slowly to 10.1 nC (R of 5 M Ω to 1 G Ω). The AC charge decreases from 21.9 nC to 0.56 nC (R of 1 k Ω to 10 M Ω) and finally to zero (R of 50 M Ω). The power matching curves calculated based on the two current outputs with different external load resistors are shown in Fig. 3e. The DC peak power density is 14.88 $\text{W}\cdot\text{m}^{-2}$ at the matching impedance of 5 M Ω , The AC peak power density is 0.13 $\text{W}\cdot\text{m}^{-2}$ at the matching

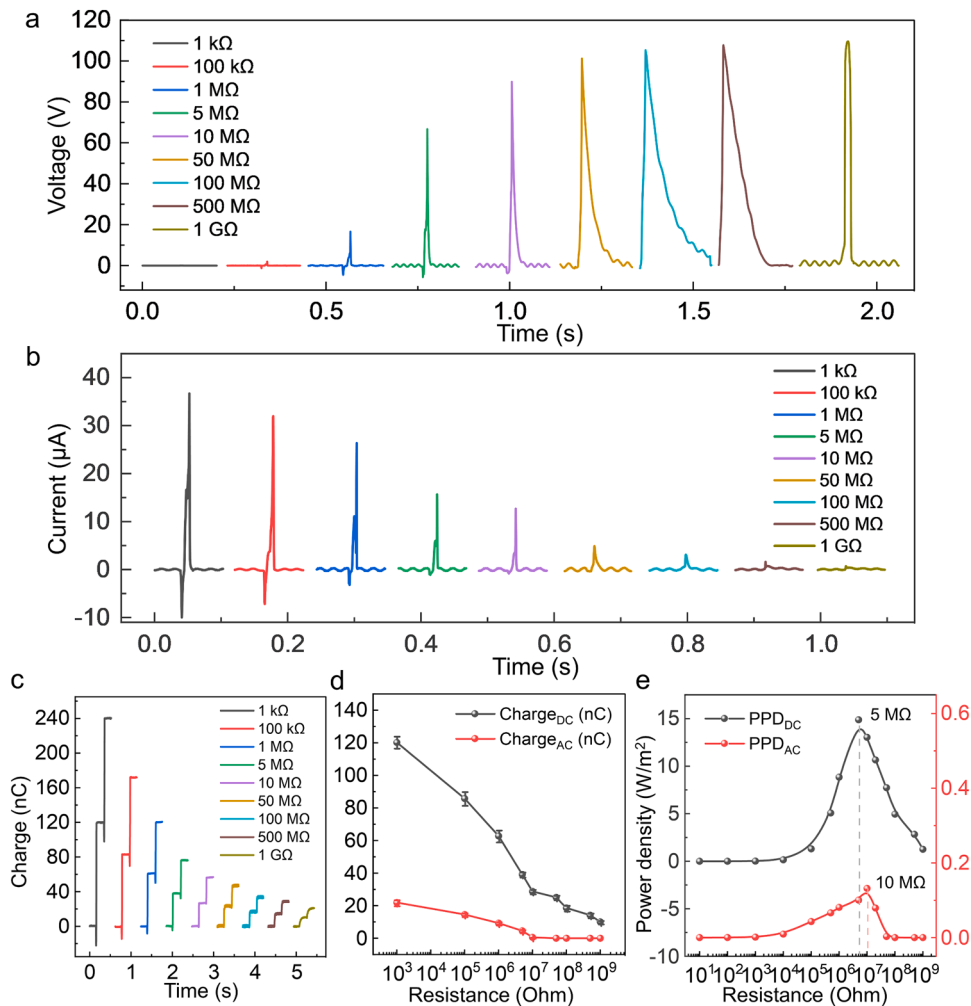


Fig. 3. Coupling characteristics under different external load resistance. (a) Voltage and (b) current on the load resistance when the heterojunction generator is connected to different external load resistances. (c) Transferred charge curves and (d) statistics of DC and AC charges, and (e) peak power density of the generator under different external load resistances.

impedance of 10 M Ω . Therefore, the DC generated by the tribovoltaic effect and the AC generated by electrostatic induction can be effectively distinguished by adjusting the external load resistance.

The normal pressure applied to the contacting interface of the heterojunction TVNG can greatly affect the devices performances, as it can influence the generated electrostatic charges and also the tribovoltaic charge excitation process. Therefore, it is intriguing to study the effect of contact pressure on electrical outputs when there is coupled tribovoltaic and electrostatic induction effects in contact-separation mode. The output variation trends of voltage and current as external force increases from 10 N to 60 N with relative humidity of 10 % are depicted in Fig. 4a and b. Correspondingly, the voltage of the TVNG is elevated from 16 V to 123 V, the DC current is elevated from 9.4 μ A to 65.6 μ A and the AC current is elevated from 4.2 μ A to 18.8 μ A. To see the periodicity of the voltage and current signals, two successive voltage/current signals are displayed in Fig. S16. The charge curve shows a step-like pattern, aligning with the increasing trend of the current (Fig. 4c). The DC charge is augmented from 38.8 nC to 198.3 nC, and the AC charge is augmented from 5.8 nC to 28.4 nC, when increasing the force from 10 to 60 N (Fig. 4d). The statistical average DC charge exhibits an approximately linear growth, whereas averaged AC charge initially rises rapidly and eventually switches to a slower growth after 30 N. As the impact force of contact-separation motion increases, the surface contact area of the two materials increases, and ultimately the contact electrification effect increases, resulting in the stronger triboelectric output. Notably, the growth rate of DC charges significantly surpasses that of AC charges. This is probably because that the contacting motion at higher impact

force could enhance the tribovoltaic charges excitation, and meantime the enlarged interface electrostatic electric field also helps enhancing the charge separation process. The effect of the normal pressure on the I - V curve shows that the built-in electric field is slightly enhanced (Fig. S17). Therefore, these two effects experience a coupled improvement to enhance the DC outputs.

2.4. Application and durability

The effect of the impact frequency on the V_{oc} and I_{sc} output is shown in Fig. S18. As frequency increases, the tribovoltaic current increases slowly, while the electrostatic current increases significantly (Fig. S19). Due to the coupling effects of contact electrification and tribovoltaic effect as well as optimized excitation parameters ($F=60$ N, $f=5$ Hz), the TVNG in this work achieves excellent open-circuit voltage and current density as compared with the output in previous literature. The DC power output of the generator is 1.49 mW with a contact area of 1 cm², which exceeds the power output of semiconductor-based generators in most previously reported literature [5,14,21,22,27,28,38–44] (Fig. 5a, b and Table S2). The comparison of electrode materials and current characteristics of contact-separation dynamic semiconductor junctions is shown in Table S3. It is found that the current output of the silicon-based homojunction and Schottky junction are both much smaller than the output of the wide-bandgap semiconductor heterojunction, because of the wide bandgap and interface electric field of the wide-bandgap semiconductor. Furthermore, the heterojunction generator maintains a stable open-circuit voltage even after 50,000 cycles,

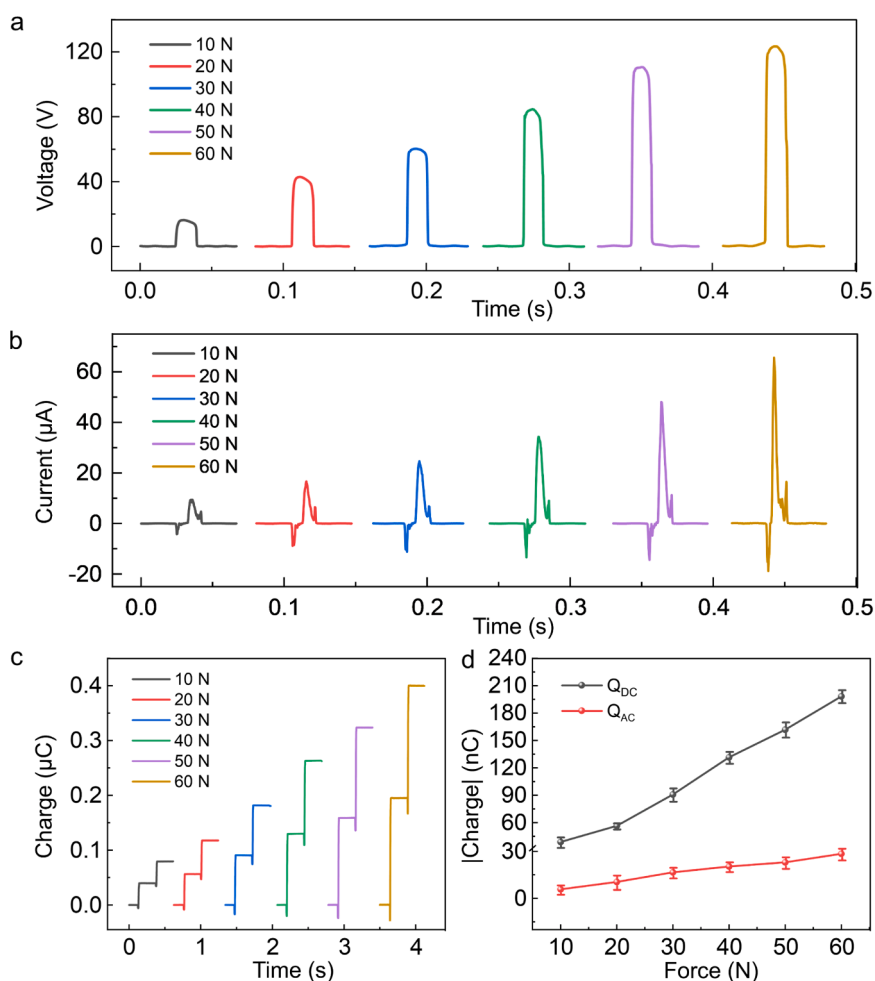


Fig. 4. Coupling characteristics under different external pressure forces. (a) Open circuit voltage and (b) short circuit current of the generator under different external pressure forces. (c) Transferred charge curves and (d) statistics of DC and AC charges under different external pressures.

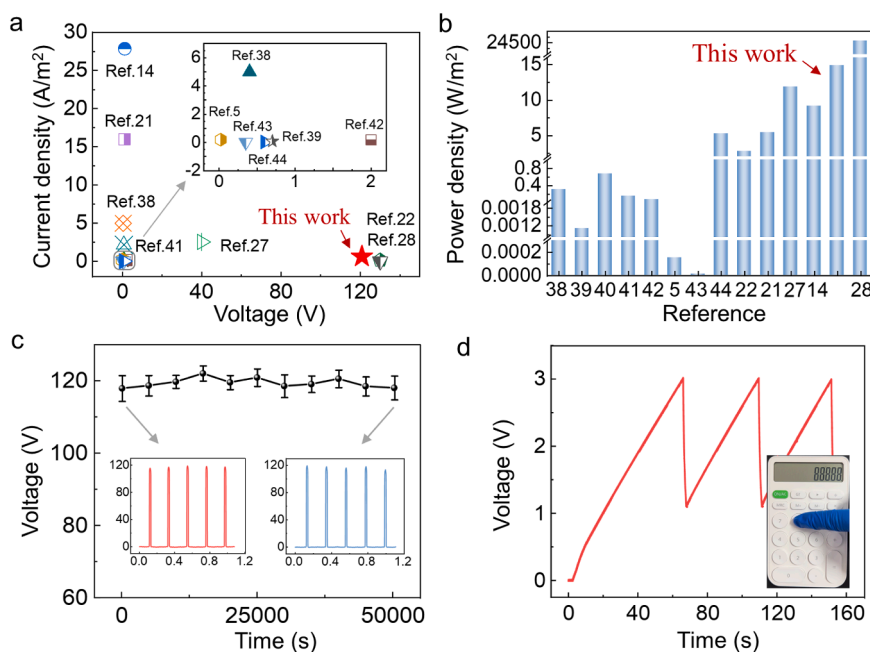


Fig. 5. Applications and durability of the heterojunction generator. Comparison of (a) open-circuit voltage and current density and (b) peak power density with various reported generators based on tribovoltaic effect. (c) Long-term durability of the generator in contact-separation mode for 50,000 cycles. (d) Voltage curve of the generator powering a commercial calculator.

demonstrating excellent durability (Fig. 5c). The original and long-term open-circuit voltage profiles after contact-separation cycling are shown in the Fig. inset, showing no noticeable degradation. A $4.7 \mu F$ capacitor is charged to 3 V by the TVNG with area of 1 cm^2 and can drives a calculator (Fig. 5d). A 3 W bulb can be lit when the $4.7 \mu F$ capacitor is charged to 5.3 V, as shown in Fig. S20. Therefore, the excellent power generation performances of the heterojunction TVNG indicates great potentials in applications of high-power mechanical energy harvesting and self-powered systems.

3. Conclusion

In summary, we investigated the coupling mechanism between the tribovoltaic and electrostatic effects of TVNG based on a dynamic heterojunction of two wide-bandgap semiconductors, i.e. zinc oxide (ZnO) and gallium nitride (GaN). We successfully examined the coupling of these two effects through the different mechanical excitation modes, environmental humidity and external load resistances. Especially, at the contact-separation mode, the DC outputs from tribovoltaic effect can be clearly distinguished from the AC outputs from the tribo-electrostatic effects. Under high humidity, surface electrostatic charge is reduced due to charge leakage, while the tribovoltaic DC outputs are less affected. The impedance matching for AC and DC currents becomes increasingly distinct with variations in external load resistance. Moreover, the increase rate in direct-current charges significantly exceeds that of alternating-current charges as external pressure is applied. Ultimately, the mechanical wearing effect can be inhibited by the contact-separation mode, achieving long-term cyclic stability over 50,000 cycles. This work could provide insights to the mechanism of tribovoltaic effects and practical guidance for high-performances tribovoltaic nanogenerators.

4. Experimental

4.1. Fabrication of the heterojunction generator

All different types of single-polish GaN wafers were purchased from China Gallium Semiconductor Technology Co., Ltd., Dongguan, China.

ZnO was purchased from Hefei Kejing Material Technology Co., Ltd., China. The diameter of the intrinsic gallium nitride (GaN) wafers is 2 in., exhibiting a characteristic growth direction of [0001]. The thicknesses of the GaN epitaxial layer, buffer layer and sapphire substrate are $4.5 \mu m$, 50 nm and 430 nm respectively. The size of the ZnO crystal substrate is $10 \text{ mm} \times 10 \text{ mm} \times 0.5 \text{ mm}$ with the crystal plane orientation of [0001], as depicted in Fig. S1 and Table S1. The crystal plane directions of the three ZnO crystal substrates are [0001], [1010] and [1120], and the size of each crystal is $5 \text{ mm} \times 5 \text{ mm} \times 0.5 \text{ mm}$. ZnO was purchased from Hefei Kejing Material Technology Co., Ltd., China. The gallium indium alloy formed good ohmic contact with the gallium nitride surface. Ag was plated on the back of ZnO as an electrode by magnetron sputtering. Double-sided Kapton tape was used to fix GaN and ZnO to acrylic plates with areas of $5 \text{ cm} \times 5 \text{ cm}$ and $1 \text{ cm} \times 1 \text{ cm}$, respectively. The acrylic plates provided stable support for friction motion.

4.2. Physical characterization and experimental measurements

Scanning electron microscopy (SEM) images of single-sided polished GaN glossy surface and ZnO crystal Zn surface were characterized using FEI Nova Nano SEM 450. Their FTIR spectra were measured by Fourier transform infrared spectrometer VERTEX80v. The X-ray diffraction patterns of ZnO single crystals and GaN samples with three crystal plane orientations were measured by XRD powder (Xpert3 Powder). The band structure was calculated from UV photoelectron spectroscopy. Ultraviolet photoelectron spectroscopy (UPS) was measured by a PHI 5000 Versa Probe III (scanning ESCA microprobe) with a He I source (21.22 eV). The current-voltage (I - V) curves of ZnO/GaN, ZnO/Ag and GaN/GaN interfaces were measured by Keithley 2450 Source Meter. In the experiments, the reciprocating motion of the generator was provided by a linear motor (GKT-37 \times 120/280 \times 360-C-SYS-SP-02). Current and voltage outputs are monitored and recorded in real time by a Keithley Electrometer 6517B. The normal force applied to the generator was measured by a dynamometer (Mark-10 M5-50, 50 lbf/800 ozF/25 kgF/25000 gF/250 N) and a digital dynamometer (ZTA-DPU-11).

Authorship statement

X.P., Z.L.W. and J.M. conceived the project and designed the experiments. J.M. and C.X.P. performed the experiments. J.M. contributed to data analysis. All authors discussed the results and commented on the manuscript. J.M., C.T.L., G.X.L., C. Z., X.P. and Z.L.W. wrote the paper with input from all authors.

CRedit authorship contribution statement

Chuntao Lan: Writing – review & editing, Visualization, Validation, Supervision, Formal analysis. **Chongxiang Pan:** Software, Methodology, Investigation, Formal analysis, Conceptualization. **Guoxu Liu:** Writing – review & editing, Validation, Supervision. **Xiong Pu:** Writing – review & editing, Project administration, Funding acquisition, Conceptualization. **Chi Zhang:** Writing – review & editing, Validation, Supervision, Funding acquisition. **Zhong Lin Wang:** Writing – review & editing, Supervision, Project administration, Funding acquisition, Conceptualization. **Jia Meng:** Writing – review & editing, Writing – original draft, Visualization, Validation, Supervision, Software, Project administration, Methodology, Investigation, Formal analysis, Data curation, Conceptualization.

Declaration of Competing Interest

The authors declare that they have no known competing financial interests or personal relationships that could have appeared to influence the work reported in this paper.

Acknowledgements

The authors thank for the support from the National Key R&D Project from Minister of Science and Technology (2021YFA1201603), National Natural Science Foundation of China (52173274, 52450006), Chinese Academy of Sciences (124GJHZ2023031MI) and the Fundamental Research Funds for the Central Universities.

Appendix A. Supporting information

Supplementary data associated with this article can be found in the online version at [doi:10.1016/j.nanoen.2024.110395](https://doi.org/10.1016/j.nanoen.2024.110395).

Data Availability

Data will be made available on request.

References

- [1] D. Zhong, C. Wu, Y. Jiang, Y. Yuan, M.-g Kim, Y. Nishio, C.-C. Shih, W. Wang, J.-C. Lai, X. Ji, T.Z. Gao, Y.-X. Wang, C. Xu, Y. Zheng, Z. Yu, H. Gong, N. Matsuhisa, C. Zhao, Y. Lei, D. Liu, S. Zhang, Y. Ochiai, S. Liu, S. Wei, J.B.H. Tok, Z. Bao, High-speed and large-scale intrinsically stretchable integrated circuits, *Nature* 627 (2024) 313–320.
- [2] S. Park, S.W. Heo, W. Lee, D. Inoue, Z. Jiang, K. Yu, H. Jinno, D. Hashizume, M. Sekino, T. Yokota, K. Fukuda, K. Tajima, T. Someya, Self-powered ultra-flexible electronics via nano-grating-patterned organic photovoltaics, *Nature* 561 (2018) 516–521.
- [3] Z.L. Wang, A.C. Wang, On the origin of contact-electrification, *Mater. Today* 30 (2019) 34–51.
- [4] M.L. Zheng, S.Q. Lin, L. Xu, L.P. Zhu, Z.L. Wang, Scanning Probing of the Tribovoltaic Effect at the Sliding Interface of Two Semiconductors, *Adv. Mater.* 32 (2020) 2000928.
- [5] Z. Zhang, D. Jiang, J. Zhao, G. Liu, T. Bu, C. Zhang, Z.L. Wang, Tribovoltaic Effect on Metal–Semiconductor Interface for Direct-Current Low-Impedance Triboelectric Nanogenerators, *Adv. Energy Mater.* 10 (2020) 1903713.
- [6] X. Yin, B.G. Xu, C.W. Kan, Y.J. Yang, Dynamic Perovskite Homo Junction Based Light-Assisted, Direct Current Tribovoltaic Nanogenerators, *Adv. Energy Mater.* 13 (2023) 2301289.
- [7] L.L. Ren, A.F. Yu, W. Wang, D. Guo, M.M. Jia, P.W. Guo, Y.F. Zhang, Z.L. Wang, J. Y. Zhai, p-n Junction Based Direct-Current Triboelectric Nanogenerator by Conjunction of Tribovoltaic Effect and Photovoltaic Effect, *Nano Lett.* 21 (2021) 10099–10106.
- [8] H.Y. Wu, J. Wang, S.K. Fu, C.C. Shan, Q.H. Zhao, K.X. Li, G. Li, Q.J. Mu, X. Wang, C.G. Hu, A constant current triboelectric nanogenerator achieved by hysteretic and ordered charge migration in dielectric polymers, *Energy Environ. Sci.* 16 (2023) 5144–5153.
- [9] Z. Zhang, L.K. Gong, R.F. Luan, Y. Feng, J. Cao, C. Zhang, Tribovoltaic Effect: Origin, Interface, Characteristic, Mechanism & Application, *Adv. Sci.* (2024) 2305460.
- [10] X. Guo, J. You, D. Wei, J. Shao, Z.L. Wang, A generalized model for tribovoltaic nanogenerator, *Appl. Phys. Rev.* 11 (2024) 021415.
- [11] M. Willatzen, Z. Zhang, Z.L. Wang, Theory of Tribovoltaics: Direct Current Generation at a p-n Semiconductor Interface, *PRX Energy* 3 (2024) 013009.
- [12] S.Q. Lin, Z.L. Wang, The tribovoltaic effect, *Mater. Today* 62 (2023) 111–128.
- [13] D. Li, C. Xu, Y.J. Liao, W.Z. Cai, Y.Q. Zhu, Z.L. Wang, Interface inter-atomic electron-transition induced photon emission in contact-electrification, *Sci. Adv.* 7 (2021) eabj0349.
- [14] J. Meng, C. Lan, C. Pan, J. Yang, X. Pu, Z.Lin Wang, Boosted outputs and robustness of polymeric tribovoltaic nanogenerator through secondary doping, *Chem. Eng. J.* 487 (2024) 150412.
- [15] Y.-S. Lee, S. Jeon, D. Kim, D.-M. Lee, D. Kim, S.-W. Kim, High performance direct current-generating triboelectric nanogenerators based on tribovoltaic p-n junction with CHCl_3 -passivated CsFAMA perovskite, *Nano Energy* 106 (2023) 108066.
- [16] F. Jiang, G. Thangavel, X. Zhou, G. Adit, H. Fu, J. Lv, L. Zhan, Y. Zhang, P.S. Lee, Ferroelectric Modulation in Flexible Lead-Free Perovskite Schottky Direct-Current Nanogenerator for Capsule-Like Magnetic Suspension Sensor, *Adv. Mater.* 35 (2023) 2302815.
- [17] L.Q. Zhang, H.F. Cai, L. Xu, L. Ji, D.A. Wang, Y.B. Zheng, Y.G. Feng, X.D. Sui, Y. F. Guo, W.L. Guo, F. Zhou, W.M. Liu, Z.L. Wang, Macro-superlubric triboelectric nanogenerator based on tribovoltaic effect, *Matter* 5 (2022) 1532–1546.
- [18] W.Y. Qiao, L.L. Zhou, Z.H. Zhao, P.Y. Yang, D. Liu, X.R. Liu, J.Q. Liu, D.Y. Liu, Z. L. Wang, J. Wang, MXene Lubricated Tribovoltaic Nanogenerator with High Current Output and Long Lifetime, *Nano-Micro Lett.* 15 (2023) 218.
- [19] H. Yuan, Z. Xiao, J. Wan, Y. Xiang, G. Dai, H. Li, J. Yang, A Rolling-Mode Al/CsPbBr₃ Schottky Junction Direct-Current Triboelectric Nanogenerator for Harvesting Mechanical and Solar Energy, *Adv. Energy Mater.* 12 (2022) 2200550.
- [20] D. Yang, L.Q. Zhang, N. Luo, Y. Liu, W.X. Sun, J.L. Peng, M. Feng, Y.E. Feng, H. F. Wang, D.A. Wang, Tribological-behaviour-controlled direct-current triboelectric nanogenerator based on the tribovoltaic effect under high contact pressure, *Nano Energy* 99 (2022) 107370.
- [21] J. Meng, C.X. Pan, L.W. Li, Z.H. Guo, F. Xu, L.Y. Jia, Z.L. Wang, X. Pu, Durable flexible direct current generation through the tribovoltaic effect in contact-separation mode, *Energy Environ. Sci.* 15 (2022) 5159–5167.
- [22] Z.Z. Wang, Z. Zhang, Y.K. Chen, L.K. Gong, S.C. Dong, H. Zhou, Y. Lin, Y. Lv, G. X. Liu, C. Zhang, Achieving an ultrahigh direct-current voltage of 130 V by semiconductor heterojunction power generation based on the tribovoltaic effect, *Energy Environ. Sci.* 15 (2022) 2366–2373.
- [23] A. Aymard, E. Delplanque, D. Dalmas, J. Scheibert, Designing metainterfaces with specified friction laws, *Science* 383 (2024) 200–204.
- [24] D. Berman, A. Erdemir, A.V. Sumant, Approaches for Achieving Superlubricity in Two-Dimensional Materials, *ACS Nano* 12 (2018) 2122–2137.
- [25] X. Xia, Z.Q. Zhou, Y.H. Shang, Y. Yang, Y.L. Zi, Metallic glass-based triboelectric nanogenerators, *Nat. Commun.* 14 (2023) 1023.
- [26] X. Huang, X. Xiang, J. Nie, D. Peng, F. Yang, Z. Wu, H. Jiang, Z. Xu, Q. Zheng, Microscale Schottky superlubric generator with high direct-current density and ultralong life, *Nat. Commun.* 12 (2021) 2268.
- [27] Z. Zhang, Z.Z. Wang, Y.K. Chen, Y. Feng, S.C. Dong, H. Zhou, Z.L. Wang, C. Zhang, Semiconductor Contact-Electrification-Dominated Tribovoltaic Effect for Ultrahigh Power Generation, *Adv. Mater.* 34 (2022) 2200146.
- [28] Z. Zhang, N. Wu, L. Gong, R. Luan, J. Cao, C. Zhang, An Ultrahigh Power Density and Ultralow Wear GaN-Based Tribovoltaic Nanogenerator for Sliding Ball Bearing as Self-Powered Wireless Sensor Node, *Adv. Mater.* 36 (2023) 2310098.
- [29] S.-K. Hong, T. Hanada, H. Makino, Y. Chen, H.-J. Ko, T. Yao, A. Tanaka, H. Sasaki, S. Sato, Band alignment at a ZnO/GaN (0001) heterointerface, *Appl. Phys. Lett.* 78 (2001) 3349–3351.
- [30] M. Grodzicki, Properties of Bare and Thin-Film-Covered GaN(0001) Surfaces, *Coatings* 11 (2021) 145.
- [31] V. Nguyen, R.S. Yang, Effect of humidity and pressure on the triboelectric nanogenerator, *Nano Energy* 2 (2013) 604–608.
- [32] S. Tu, T. Tian, T. Xiao, X. Yao, S. Shen, Y. Wu, Y. Liu, Z. Bing, K. Huang, A. Knoll, S. Yin, S. Liang, J.E. Heger, G. Pan, M. Schwartzkopf, S.V. Roth, P. Müller-Buschbaum, Humidity Stable Thermoelectric Hybrid Materials Toward a Self-Powered Triple Sensing System, *Adv. Funct. Mater.* (2024) 2316088.
- [33] Y.Q. Hu, X.L. Wang, H.K. Li, H.Q. Li, Z.H. Li, Effect of humidity on tribological properties and electrification performance of sliding-mode triboelectric nanogenerator, *Nano Energy* 71 (2020) 104640.
- [34] Q.Z. Sun, F. Liang, G.Z. Ren, L.R. Zhang, S.H. He, K. Gao, Z.Y. Gong, Y.L. Zhang, X. Kang, C.C. Zhu, Y.X. Song, H.X. Sheng, G. Lu, H.D. Yu, W. Huang, Density-of-States Matching-Induced Ultrahigh Current Density and High-Humidity Resistance in a Simply Structured Triboelectric Nanogenerator, *Adv. Mater.* 35 (2023) 2210915.
- [35] Z. Chen, X. He, C. Xiao, S. Kim, Effect of Humidity on Friction and Wear—A Critical Review, *Lubricants* 6 (2018) 74.
- [36] Y.L. Zi, S.M. Niu, J. Wang, Z. Wen, W. Tang, Z.L. Wang, Standards and figure-of-merits for quantifying the performance of triboelectric nanogenerators, *Nat. Commun.* 6 (2015) 8376.

- [37] S.X. Li, S. Deng, R. Xu, D. Liu, Y. Nan, Z.W. Zhang, Y.K. Gao, H.F. Lv, M. Li, Q. Zhang, J. Wang, Z.L. Wang, High-Frequency Mechanical Energy Harvester with Direct Current Output from Chemical Potential Difference, *ACS Energy Lett.* 7 (2022) 3080–3086.
- [38] J. Liu, M.M. Miao, K.R. Jiang, F. Khan, A. Goswami, R. Mcgee, Z. Li, L. Nguyen, Z. Y. Hu, J. Lee, K. Cadien, T. Thundat, Sustained electron tunneling at unbiased metal-insulator-semiconductor triboelectric contacts, *Nano Energy* 48 (2018) 320–326.
- [39] J. Meng, Z.H. Guo, C.X. Pan, L.Y. Wang, C.Y. Chang, L.W. Li, X. Pu, Z.L. Wang, Flexible Textile Direct-Current Generator Based on the Tribovoltaic Effect at Dynamic Metal-Semiconducting Polymer Interfaces, *ACS Energy Lett.* 6 (2021) 2442–2450.
- [40] R.Z. Yang, M. Benner, Z.P. Guo, C. Zhou, J. Liu, High-Performance Flexible Schottky DC Generator via Metal/Conducting Polymer Sliding Contacts, *Adv. Funct. Mater.* 31 (2021) 2103132.
- [41] H. Shao, J. Fang, H.X. Wang, L.M. Dai, T. Lin, Polymer-Metal Schottky Contact with Direct-Current Outputs, *Adv. Mater.* 28 (2016) 1461–1466.
- [42] U. Liu, M.I. Cheikh, R.M. Bao, H.H. Peng, F.F. Liu, Z. Li, K.R. Jiang, J. Chen, T. Thundat, Tribo-Tunneling DC Generator with Carbon Aerogel/Silicon Multi-Nanocontacts, *Adv. Electron. Mater.* 5 (2019) 1900464.
- [43] R. Xu, Q. Zhang, J.Y. Wang, D. Liu, J. Wang, Z.L. Wang, Direct current triboelectric cell by sliding an n-type semiconductor on a p-type semiconductor, *Nano Energy* 66 (2019) 104185.
- [44] S.S. Lin, Y.H. Lu, S.R. Feng, Z.Z. Hao, Y.F. Yan, A High Current Density Direct-Current Generator Based on a Moving van der Waals Schottky Diode, *Adv. Mater.* 31 (2019) e1804398.